coatings

MDPI

Article

Effect of Cooling Method on Microstructure and Microhardness of CuCrFeMnNi High-Entropy Alloy

Yajun Zhou [1], Ruifeng Zhao [2,*], Hechuan Geng [1], Bo Ren [1,3,*], Zhongxia Liu [1], Jianxiu Liu [1], Aiyun Jiang [1] and Baofeng Zhang [1]

[1] Faculty of Engineering, Huanghe Science and Technology College, Zhengzhou 450061, China; hkdzyj@163.com (Y.Z.); 17513286184@163.com (H.G.); liuzhongxia@zzu.edu.cn (Z.L.); jianxiuliu@hhstu.edu.cn (J.L.); aiyunjiang@126.com (A.J.); zhangbf1979@163.com (B.Z.)
[2] School of Science, Henan University of Engineering, Zhengzhou 450001, China
[3] School of Mechanical Engineering, Henan University of Engineering, Zhengzhou 450001, China
* Correspondence: zrf193513@163.com (R.Z.); renbo193513@163.com (B.R.)

Abstract: This study investigated four cooling methods for CuCrFeMnNi high-entropy alloy, namely, furnace cooling, air cooling, oil cooling, and water cooling (designated as FC, AC, OC, and WC, respectively), following a 12 h treatment at 800 °C. Results indicate that all four cooled alloys consisted of two FCC solid-solution phases (FCC1 and FCC2) and ρ phases. However, the FC alloy primarily contained FCC2 as the main phase and FCC1 as the secondary phase. The other three cooling methods yielded alloys with FCC2 as the primary phase and FCC1 as the secondary phase. With an increase in cooling rate, the content of the FCC1 phase gradually increased, that of the ρ phase initially decreased and then increased, and that of the FCC2 phase gradually decreased. The microstructure of the CuCrFeMnNi high-entropy alloy under the four cooling methods consisted of gray-black dendrites rich in Cr-Fe and white dendrites rich in Cu. Black ρ-phase particles predominated the dendrite region. As the cooling rate increased, the white interdendritic regions shrank, and the gray-black interdendritic regions expanded. The FC alloy exhibited the lowest microhardness at approximately 202.6 HV. As the cooling rate increased, the microhardness of the alloy progressively increased. The microhardness of the WC alloy was the highest, at approximately 355 HV. The strengthening mechanisms for all the alloys were primarily solid-solution strengthening and second-phase precipitation strengthening.

Keywords: cooling method; high-entropy alloy; microstructure; microhardness

Citation: Zhou, Y.; Zhao, R.; Geng, H.; Ren, B.; Liu, Z.; Liu, J.; Jiang, A.; Zhang, B. Effect of Cooling Method on Microstructure and Microhardness of CuCrFeMnNi High-Entropy Alloy. *Coatings* **2024**, *14*, 831. https://doi.org/10.3390/coatings14070831

Academic Editors: Ben Beake and Michał Kulka

Received: 27 May 2024
Revised: 23 June 2024
Accepted: 1 July 2024
Published: 3 July 2024

1. Introduction

High-entropy alloys (HEAs) are composed of four or more metallic elements whose atomic percentages range from 5 at.% to 35 at.%. This new type of alloy forms simple solid-solution phases. Following the introduction of this concept by Yeh [1] and Cantor [2], the HEA design was recognized by Ranganathan [3] as one of the three major advancements in modern metal science. The superior characteristics of HEAs, which set them apart from traditional alloys, are primarily attributed to their long-range ordered and short-range disordered structures [4]. Despite the complex chemical composition of HEAs, most of them maintain a primary phase of simple solid solutions (such as FCC, BCC, and HCP) [5–10]. However, these solid solutions are not always stable; they may enter a substable phase during specific composition or preparation processes, leading to phase decomposition, transformation, or precipitation, all of which significantly affect the microstructure and properties of the alloys [11–14]. Therefore, studying the phase stability of HEAs under various conditions is critical.

The microstructure of most HEAs can be optimized by heat treatment, thereby improving their mechanical properties. Chen et al. [15] annealed $Al_xCrFe_{1.5}MnNi_{0.5}$ (x = 0.3, 0.5) HEAs at 500 °C–900 °C, and found that the BCC phase partially transformed into a

tetragonal ρ ($Cr_5Fe_6Mn_8$) phase resulting in a hardness of over 950 HV. Tsao et al. [16] quenched $Al_{0.3}CrFe_{1.5}MnNi_{0.5}$ HEAs after heat treatment at 650 °C–75 °C for 8 h and found that the microstructure exhibited precipitated AlNi and $Cr_5Fe_6Mn_8$ phases in the matrix dendrites after aging at 650 °C. Meanwhile, the β1 FCC phase between dendrites decomposed into the matrix structure and transformed into a second phase (β2 FCC) after aging at 750 °C. Owing to the precipitation of the Ni-rich, Al-rich, and $Cr_5Fe_6Mn_8$ phases, the hardness of the alloy was remarkably improved. Ren's research [17] showed that the $CuCr_2Fe_2NiMn$ alloy prepared using an arc melting process composed of two FCC phases (FCC1 and FCC2) plus a minor amount of $Cr_5Fe_6Mn_8$ phase underwent age hardening after aging at 800 °C for 12 h, with its microhardness increasing from 334 HV in the as-cast state to 450 HV. However, after aging at 950 °C and 1100 °C for 12 h, significant age softening occurred and the microhardness decreased to 180 HV. The age hardening was attributed to the metastable BCC phase that precipitated the ρ phase of hard intermetallic compounds at low temperatures (600 °C–800 °C), thus significantly improving the hardness of the alloy. Further increasing the aging temperature resulted in the partial decomposition of the ρ phase at 950 °C and its complete decomposition at 1100 °C, leading to a sharp decrease in the microhardness of the alloy.

Zhao et al. [18] and Ren et al. [19] prepared CrCuFeMnNi HEA powder, consisting of an FCC main phase and a BCC secondary phase, by mechanical alloying. After vacuum annealing between 700 and 900 °C, the phase structure transformed into two FCC phases (FCC1 and FCC2), a minor BCC phase, and a minor $Cr_5Fe_6Mn_8$ phase [18]. After vacuum hot-press sintering at 950 °C and 50 MPa for 2 h, the alloy-phase structure transformed into two FCC phases (FCC1 and FCC2) and a small amount of BCC and ρ phases. Mohanty et al. [20,21] prepared AlCoCuNiZn HEA by powder metallurgy and subjected it to solid solution + aging treatment. They also studied the effect of aging treatment on the microstructure and microhardness of the alloy and found that the alloy sintered at 950 °C consisted of β (FCC) and α (L12) phases. After solid-solution treatment at 1160 °C for 96 h, the phase structure of the alloy completely transformed into a single α (L12) phase. After aging treatment at 400 °C–1000 °C for 48 h and quenching in ice water, the alloy reached peak age hardening (~633 HV) at 500 °C, which was almost equivalent to its sintered hardness (~625 HV). This study proves that spark plasma sintering (SPS) has sintering aging effects, resulting in the high hardness of the sintered alloy. The cooling method after the heat treatment also affects the microstructure and properties of HEAs. Yao et al. [22] studied the effect of the cooling method on the precipitation of secondary phases and the mechanical properties of CoCrFeMnNi–$Mo_5C_{0.5}$ HEA and found that with an increase in cooling rate, the hardness of the HEA decreased and its uniform plastic deformation and elongation increased. The research of Xiong et al. [23] showed that the cooling rate could change the phase composition and shape of$Al_{0.5}$CoCrFeNi HEA from the BCC+FCC phase to the BCC+FCC+B2 phase, and the BCC phase transformation was coarse. The ultimate tensile strength and yield strength of the alloy after heat treatment decreased with the increase in cooling rate, but the elongation and Vickers hardness increased with the increase in cooling rate. Yu et al. [24] used liquid nitrogen and water as the cooling medium to study the evolution of microstructure and mechanical properties of $Co_{35}Cr_{25}Fe_{37.5}Ni_{2.5}$ dual-phase HEA. Compared with water cooling, after liquid nitrogen cooling, a large number of HCP-phase laminates with different lengths and thicknesses intersected in the grain, and the HCP-phase area fraction was multiplied, resulting in the alloy still having a yield strength of 482 MPa and an ultimate tensile strength of 1079 MPa after 900 °C annealing.

These studies suggest that under specific conditions, the metastable phase of as-cast alloys undergoes phase transformation, leading to age hardening or softening. Mechanically alloyed HEA powders typically consist of a supersaturated solid solution. When subjected to plasma or vacuum hot-press sintering with high temperatures, pressures, and prolonged heat treatment, these alloys achieve a more stable phase structure compared with cast alloys [25,26]. However, subsequent solid-solution or aging conditions may still induce phase transformations, resulting in age hardening or softening. To gain a deep un-

derstanding of the microstructural and mechanical changes in vacuum hot-pressed HEAs during subsequent heat treatments, this study focused on the CuCrFeMnNi HEA produced by vacuum hot-press sintering. The alloy was subjected to isothermal aging, followed by treatments including furnace cooling, room-temperature cooling, water cooling, and oil cooling. This work aimed to investigate how these cooling methods impacted the alloy's phase structure, microstructure, elemental distribution, and microhardness.

2. Materials and Methods

CuCrFeMnNi HEA was synthesized using powder metallurgy. This process was primarily divided into two steps: first, the alloy powder was produced using mechanical alloying according to the stoichiometric ratio of CuCrFeMnNi [18]. The high-purity (>99.9%) Cu, Cr, Fe, Mn, and Ni elemental powders used in the experiment were provided by Beijing Guanjinli New Material Co., Ltd. (Guanjinli New Material Co., Ltd, Beijing, China), and the particle size of each powder was about 75 μm. We weighed the powders according to the equal molar ratio and put them into a stainless-steel ball-mill tank, and then added stainless-steel balls at a ball-to-powder ratio of 10:1. After the ball-mill tank was assembled, it was washed with high-purity argon for 5 min. Finally, it was mechanically ball milled on a QM-WX4 ball mill (Nanjing Dongmai Technology Instrument Co., Ltd, Nanjing, China) with a speed of 300 rpm and a time of 45 h dry grinding + 5 h wet grinding. An appropriate amount of anhydrous ethanol was injected into the stainless-steel tank during the wet grinding. The powder, after wet grinding, was dried in a vacuum drying oven at 50 °C for 3 days, and finally, the alloy powder was sieved by a 75 μm stainless-steel sieve. Secondly, the bulk CuCrFeMnNi high-entropy alloy was prepared in a ZT-25-20YVHP vacuum hot-press sintering furnace (Shanghai Chenhua Technology Co., Ltd, Shanghai, China) [19]. When hot-press sintering, the background vacuum was 1×10^{-3} Pa, the heating rate was 15 °C/min, the sintering temperature was 950 °C, the sintering pressure was 50 MPa, and the holding time was 2 h. After cooling in the furnace, a cylindrical sample of Æ12.5 mm × 6 mm was obtained. A bulk of Æ12.5 mm × 6 mm was then prepared by hot-press sintering [19]. The alloy was processed into thin-sheet samples with dimensions of Φ12.5 mm × 2 mm using wire cutting and then heat-treated in a box-type resistance furnace (Shenzhen Liangyi Laboratory Instrument Co., Ltd, Shenzhen, China). The heat treatment protocol involved maintaining the temperature at 800 °C for 12 h, followed by cooling through four methods: furnace cooling, air cooling, oil (mineral oil) cooling, and water (room-temperature) cooling (designated as FC, AC, OC, and WC, respectively). For furnace cooling, we turned off the power supply to cease heating, allowing the sample to cool in the furnace to room temperature before removal. For air cooling, the sample was removed from the furnace, placed on the cement floor, and allowed to cool naturally to room temperature. In oil and water cooling, the samples were removed from the furnace and immersed in mineral oil (~25°C) or water (~25°C), respectively, for 10 min before removal. The cooling rates for the four different cooling methods were [23]: 0.02~0.03 °C/s (FC), 0.9~1.8 °C/s (AC), >20 °C/s (OC), and >75 °C/s (WC).

The microstructure and hardness of the four HEAs after heat treatment were characterized using SiC abrasive-paper grinding and diamond polishing paste. Analysis was conducted using X-ray diffraction (XRD, Bruker D8 ADVANCE) (Bruker, Billerica, MA, USA) and scanning electron microscopy (SEM, Quanta 250) (FEI Company, Hillsboro, OR, USA). X-ray measurements were performed using Cu-Kα radiation with a wavelength of 1.54056 Å. The operating tube voltage and current were set at 40 kV and 40 mA, respectively, and the scanning angle, speed, and step size were 20°–90° (2θ), 5°/min, and 0.02°, respectively. The HEA composition was analyzed using the SEM's built-in electron energy spectrometer (EDAX). The hardness of the HEA was measured using the HVS-50 microhardness tester (Changzhou Sanfeng Instrument Technology Co., Ltd, Changzhou, China) at an applied load of 98 N and a holding time of 20 s. Each sample was tested five times to determine the average hardness of the alloy.

3. Results and Discussion

3.1. XRD Analysis

The XRD patterns of the CuCrFeMnNi HEA under four cooling methods are presented in Figure 1. The alloys were composed of two FCC solid solutions (FCC1 and FCC2) and two phases. In particular, the furnace-cooled (FC) alloy had FCC2 as its primary phase and FCC1 as its secondary phase. The other three cooling methods produce alloys with FCC2 as the primary phase and FCC1 as the secondary phase. Formula (1) can be used to estimate the relative content of each phase for the CuCrFeMnNi HEA under these four cooling methods, as listed in Table 1 [18,19].

$$RC_a = \frac{\sum I_{i(a)}}{\sum I_{i(a)} + \sum I_{i(b)} + \cdots} \times 100\% \quad (1)$$

where RC_a is the relative volume fraction (or relative content) of phase A in the bulk alloy, and $I_{i(a)}$ and $I_{i(b)}$ are the relative intensities of the ith diffraction peak of phases A and B in the XRD spectrum.

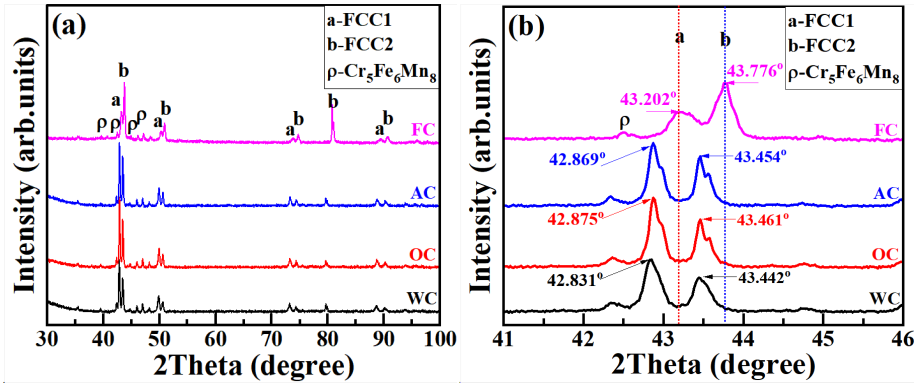

Figure 1. XRD patterns of the CuCrFeMnNi HEA under four cooling modes: (**a**) 30°–90° and (**b**) 41°–46°.

Table 1. Relative content of each phase of the CuCrFeMnNi HEA under four cooling methods.

Cooling Methods	Relative Content (%)		
	FCC1	FCC2	ρ
FC	27.4	52.2	20.4
AC	47.6	37.6	14.8
OC	50.1	34.6	15.3
WC	51.3	32.3	16.4

CuCrFeMnNi HEA powder consists of a metastable FCC main phase and a BCC secondary phase [18,19]. In the sintered state, these phases transform into the FCC1 main phase, the FCC2 secondary phase, and a ρ phase with relative contents of 40.2%, 31.8%, and 28.0%, respectively. When the furnace was cold, the relative content of the FCC1 phase decreased to 27.4%, that of the FCC2 phase increased to 52.2%, and that of the ρ phase decreased to 20.4%. With an increase in cooling rate, the relative content of the FCC1 phase increased from 27.4% to 51.3%, that of the FCC2 phase decreased from 52.2% to 32.3%, and that of the ρ phase initially decreased from 20.4% to 14.8%, and then slightly increased to 16.4%. This finding indicates that during high-temperature heat treatment, the precipitation and decomposition of these phases occurs dynamically [18]. In particular, the high-melting-point phases preferentially precipitate during cooling [27]. The ρ phase is a $Cr_5Fe_6Mn_8$ intermetallic compound with a tetragonal crystal structure and is known for its relatively high melting point. Its primary constituents are Cr, Fe, and Mn, and it exhibits

high microhardness (1273 HV). In XRD, it is primarily observed in the range of 2θ = 41° to 49° [15]. FCC1 is an (Fe, Cr, Mn)-rich phase, with a lower melting point than the ρ phase, and FCC2 is a (Cu, Ni, Mn)-rich phase, with the lowest melting point. The differing lattice constants of the two phases resulted in a double-peak phenomenon in the XRD patterns. The CuCrFeMnNi sintered alloy underwent isothermal aging and four different cooling methods. The phases comprised two types of FCC phase (FCC1 and FCC2) plus a minor amount of the $Cr_5Fe_6Mn_8$ phase, closely resembling previous research findings.

At low cooling rates (FC state), Cu, Mn, and Ni were at high concentrations and had similar lattice types, allowing ample time for the solid solution and formation of the FCC2 phase and leading to the high FCC2 content. Meanwhile, some of the FCC1 phase decomposed into the ρ phase, resulting in a lower content of the FCC1 phase and a higher content of the ρ phase. However, at high cooling rates (WC state), the high-melting-point ρ phase and the FCC1 phase precipitated before decomposition, resulting in their high relative contents.

As shown in Figure 1b, the main peaks of the FCC1 and FCC2 phases in the heat-treated alloy shifted to small angles with the increasing cooling rate. At low cooling rates (FC state), each element diffused sufficiently to form FCC1, FCC2, and ρ phases. The main solid-solution element of the FCC1 phase was Cr-Fe, the main solid-solution element of the FCC2 phase was Cu-Ni, and the main component of the ρ phase was Cr-Fe-Mn. At high cooling rates (AC, OC, and WC states), both the FCC2 phase and the ρ phase content decreased, indicating that alloying elements in the FCC2 phase and ρ phase diffused with each other, leading to an increase in the FCC1 phase content. Among these alloying elements, the atomic radii in descending order were Mn>Cu>Cr>Ni>Fe. The Mn element caused by the decomposition of the ρ phase diffused into FCC1 and FCC2, resulting in an increase in their lattice constants. Therefore, the main peaks of FCC1 and FCC2 phases in XRD shifted towards a small angle direction. Yao et al. [22] observed a similar phenomenon in their study of the CoCrFeMnNi-$Mo_5C_{0.5}$ alloy: the FCC phase diffraction peaks also shifted to small angles with an increase in the cooling rate.

3.2. Microstructure

Figure 2 shows the SEM images of the CuCrFeMnNi HEA under the four cooling conditions. The microstructures of all four alloys exhibited dendritic (DR, purple) and interdendritic (ID, black) morphologies, with white particles predominantly located in the dendritic regions. As the cooling rate increased, the purple interdendritic regions shrank and the black dendritic regions expanded.

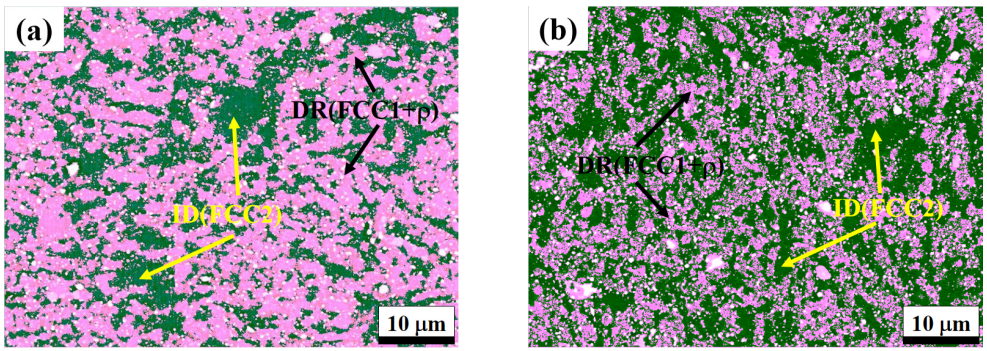

Figure 2. *Cont.*

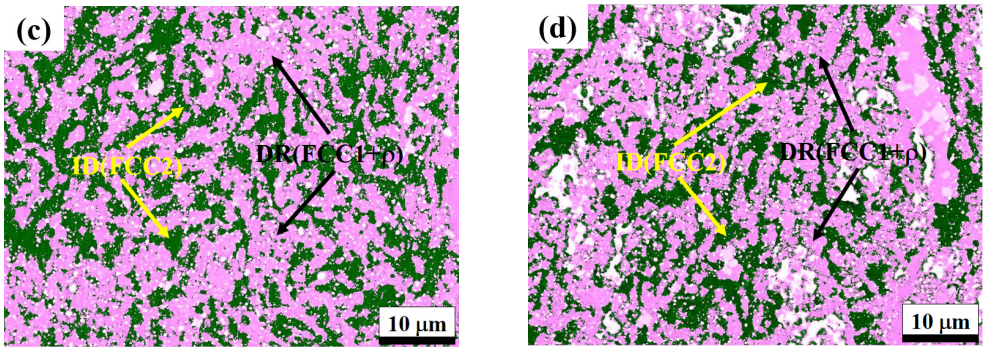

Figure 2. SEM images of the CuCrFeMnNi HEA under four cooling methods: (**a**) FC, (**b**) AC, (**c**) OC. and (**d**) WC.

Figure 3 illustrates the SEM map scanning results of the CuCrFeMnNi HEA after furnace cooling. Figure 3 reveals that the main element in the white interdendritic region (zone B) was Cu. Meanwhile, the main elements in the gray interdendritic region (zone A) were Cr and Fe, with relatively even distributions of Ni and Mn. Figures 4–6 present the SEM surface scanning results of the CuCrFeMnNi HEA after air, oil, and water cooling, respectively. The microstructure of these alloys was similar to that of the FC alloy. The gray interdendritic region (zone A) was rich in Cr-Fe, and the white interdendritic region (zone B) was rich in Cu. Table 2 lists the results from the EDS analysis of the microstructure of the CuCrFeMnNi HEA under the four cooling methods. All four alloys exhibited compositional segregation, with the DR region being rich in Cr-Fe and the ID region being rich in Cu. EDS analysis of the black particles in Figures 3–6 indicated that they primarily consisted of Cr, Fe, and Mn. In conjunction with XRD analysis, this finding indicates that the DR region in these alloys represented the Cr-rich FCC1 phase, the ID region represented the Cu-rich FCC2 phase, and the black particles (zone C) represented the ρ phase.

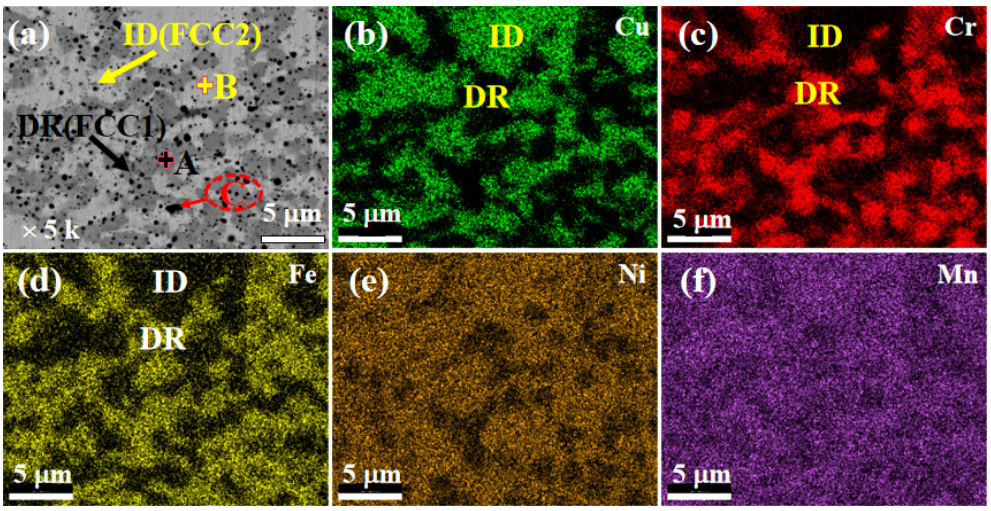

Figure 3. SEM map scanning results of the CuCrFeMnNi HEA after FC state: (**a**) backscatter image, (**b**) Cu, (**c**) Cr, (**d**) Fe, (**e**) Ni, and (**f**) Mn.

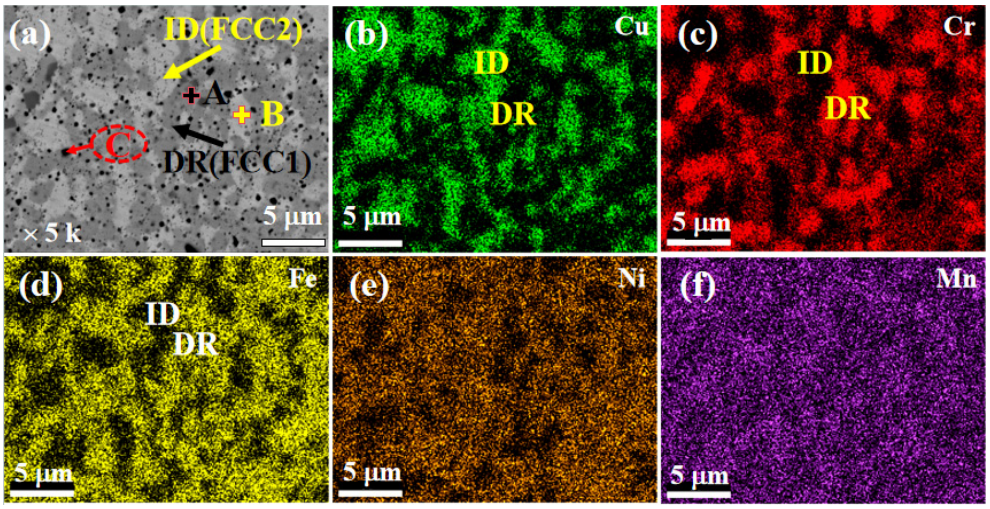

Figure 4. SEM map scanning results of CuCrFeMnNi HEA after AC state: (**a**) backscatter image, (**b**) Cu, (**c**) Cr, (**d**) Fe, (**e**) Ni, and (**f**) Mn.

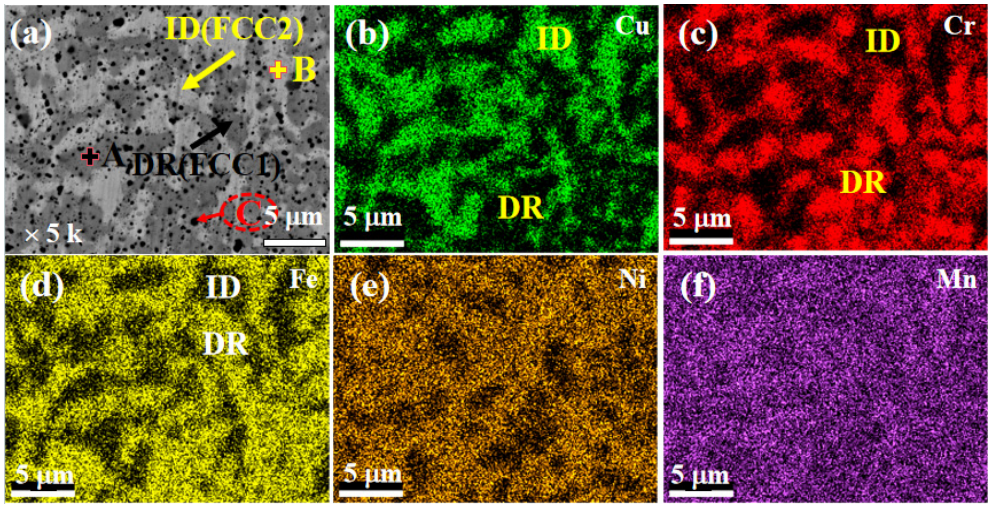

Figure 5. SEM map scanning results of CuCrFeMnNi HEA after OC state: (**a**) backscatter image, (**b**) Cu, (**c**) Cr, (**d**) Fe, (**e**) Ni, and (**f**) Mn.

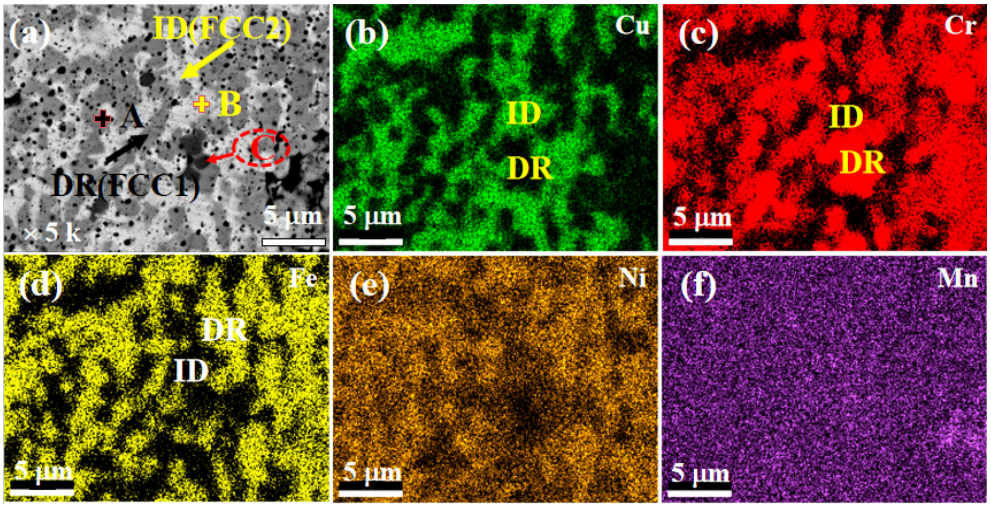

Figure 6. SEM map scanning results of CuCrFeMnNi HEA after WC state: (**a**) backscatter image, (**b**) Cu, (**c**) Cr, (**d**) Fe, (**e**) Ni, and (**f**) Mn.

Table 2. EDS analysis of the microstructure of the CuCrFeMnNi HEA under the four cooling methods.

Sample	Point	Cu	Cr	Fe	Mn	Ni
FC	A	9.7	30.3	27.4	16.2	16.4
	B	34.2	8.8	11.0	23.1	22.9
	C	16.4	17.6	21.3	28.1	16.6
AC	A	5.1	33.5	28.8	12.5	20.1
	B	32.4	8.2	14.7	22.8	21.9
	C	14.9	18.2	21.6	30.6	14.7
OC	A	10.2	35.4	25.8	13.6	15
	B	29.4	12.5	13.9	21.3	22.9
	C	14.5	19.3	23.2	31.2	11.8
WC	A	7.2	36.6	27.4	11.9	16.9
	B	39.5	4.4	5.1	28	23
	C	14.9	19.1	22.4	31.2	12.4

Figure 3 illustrates the SEM map scanning results of CuCrFeMnNi HEA after furnace cooling. Figure 3 reveals that the dark-gray area (Zone A) was a dendritic region (DR), with the main elements being Cr, Fe, Ni, and Mn. The gray-white area (Zone B) was the interdendritic region (ID), with the main elements being Cu, Ni, and Mn. In the DR region of Figure 3a, black particles with sizes of several micrometers or hundreds of nanometers can be observed, and EDS results confirm that their main components were Cr, Fe, and Mn. Overall, the segregation of Cu, Cr, and Fe elements was more severe, while the distribution of Ni and Mn elements was relatively uniform. Figures 4–6 show the SEM and elemental map scanning results of CuCrFeMnNi HEA in AC, OC, and WC states, respectively. In the three states, the microstructure of the alloy was similar to that of the FC-state alloy. The main elements in the dark-gray DR region (A region) were Cr, Fe, Ni, and Mn, while the main elements in the gray-white ID region (B region) were Cu, Ni, and Mn. The main components of the black particles dispersed in the DR region were still Cr, Fe, and Mn. Table 2 presents the EDS analysis results of the microstructure of CuCrFeMnNi HEA under four cooling methods. It can be seen that the elemental content of points A, B, and C in each alloy was consistent with the map scanning results. Based on the XRD analysis results in Figure 1, it can be inferred that the DR region in the alloy under the four cooling methods was the FCC1 phase rich in Cr-Fe-Ni-Mn, the ID region was the FCC2 phase rich in Cu-Ni-Mn, and the black particles (C region) were the ρ phase.

3.3. Hardness

Figure 7 illustrates the microhardness of the CuCrFeMnNi HEA under the four cooling methods. The FC alloy yielded a microhardness of approximately 202.6 HV, which then gradually increased with the cooling rate. WC resulted in the highest microhardness of 355 HV. Zhao et al. [28] found that in the sintered state, the microstructure of CuCrFeMnNi HEA comprised an FCC1 phase rich in Cr-Fe, an FCC2 phase rich in Cu, and a ρ phase. Its microhardness reached 543 HV. However, the present study found that after heat treatment at 800 °C for 12 h, the phase structure remained unchanged but the main phase transition was from FCC1 to FCC2, with a significant reduction in the relative content of the ρ phase. Zhao et al. [28] also reported that the FCC1 phase was harder than the FCC2 phase, the ρ phase also had high hardness, and their decreased relative content primarily led to a reduction in the alloy's microhardness. With an increase in the cooling rate, the alloy's phase structure shifted from FCC2 to FCC1, accompanied by a relative increase in the phase content. This phenomenon resulted in an increase in microhardness. Compared with AC- and OC-state alloys, the cooling rate of WC-state alloy was faster, and the relative content of hard phases FCC1 and ρ in the alloy was the highest, so its microhardness was the highest, reaching 355 HV. These results show that the strengthening mechanisms of the WC-state alloy were primarily solid-solution strengthening and second-phase precipitation strengthening.

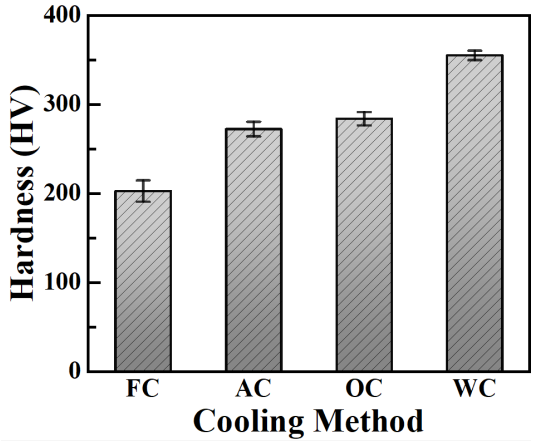

Figure 7. Microhardness of CuCrFeMnNi HEA under the four cooling methods.

4. Conclusions

In this work, CuCrFeMnNi HEA was heat-treated at 800 °C for 12 h, followed by FC, AC, OC, or WC. The microstructure and microhardness of the alloy were analyzed by XRD, SEM, EDS, and microhardness tester. All four alloys were composed of two types of FCC solid solution (FCC1 and FCC2) and ρ phases. However, the FC-state alloy contained FCC2 as its primary phase and FCC1 as its secondary phase. Meanwhile, the alloys cooled by the other three methods had FCC2 as their primary phase and FCC1 as their secondary phase. As the cooling rate increased, the content of the FCC1 phase gradually increased, that of ρ phase first decreased and then increased, and that of FCC2 phase gradually decreased. The microstructure of CuCrFeMnNi HEA under the four cooling modes was composed of gray-black dendrites rich in Cr-Fe and white interdendrites rich in Cu, with black ρ-phase particles predominantly located in the dendritic region. With an increase in the cooling rate, the white interdendritic region shrank and the gray-black interdendritic region gradually expanded. The microhardness of the FC-state alloy was the lowest at approximately 202.6 HV. As the cooling rate increased, the microhardness of the alloy progressively increased. The microhardness of the WC-state alloy was the highest at approximately 355 HV. The strengthening mechanisms of these alloys were primarily solid-solution strengthening and second-phase precipitation strengthening.

Author Contributions: Methodology, B.R. and Y.Z.; investigation, B.R., R.Z. and A.J.; resources, H.G.; data curation, J.L.; writing—original draft preparation, B.R.; writing—review and editing, R.Z., Z.L. and B.Z.; project administration, B.R. and Y.Z.; funding acquisition, R.Z., B.R. and H.G. All authors have read and agreed to the published version of the manuscript.

Funding: This research was funded by the Key Scientific Research Project Plan of Colleges and Universities in Henan Province, Grant No. 22A430014; the Henan Province Science and Technology Research Plan Project, Grant No. 232102231007, the 2023 College Student Innovation and Entrepreneurship Training Program, Grant No. 202311834042; the Young Backbone Teacher Training Program of Henan Province Colleges and Universities, Grant No. 2020GGJS271; and the Zhengzhou Basic Research and Applied Basic Research Special Fund Project, Grant No. ZZSZX202105.

Institutional Review Board Statement: Not applicable.

Informed Consent Statement: Not applicable.

Data Availability Statement: Data are contained within the article.

Conflicts of Interest: The authors declare no conflicts of interest.

References

1. Yeh, J.W.; Chen, S.K.; Lin, S.J.; Can, J.Y.; Chin, T.S.; Shun, T.T.; Tsau, C.H.; Chang, S.Y. Nanostructured high entropy alloys with multiple principal elements: Novel alloy design concepts and outcomes. *Adv. Eng. Mater.* **2004**, *6*, 299–303. [CrossRef]
2. Cantor, B.; Chang, I.T.H.; Knight, P.; Vincent, A.J.B. Microstructure development in equiatomic multicomponent alloys. *Mater. Sci. Eng. A* **2004**, *375–377*, 213–218. [CrossRef]
3. Ranganathan, S. Alloyed pleasures: Multimetallic cocktails. *Curr. Sci.* **2003**, *85*, 1404–1406.
4. Yang, X.; Zhang, Y. Prediction of high-entropy stabilized solid-solution in multi-component alloys. *Mater. Chem. Phys.* **2012**, *132*, 233–238. [CrossRef]
5. Gu, Z.; He, J.Y.; Qin, Y.B.; Zhang, P.; Zhang, P.C.; Zhang, D.L.; Wu, H.J.; Xiao, L.L.; Xi, S.Q. Ultra strong FCC structured $Ni_8Cr_4Co_4Fe_6W_2$ high entropy alloys with high strength and ductility by laser powder bed fusion. *J. Alloys Compd.* **2024**, *992*, 74580. [CrossRef]
6. Guo, X.P.; Guo, Y.Q.; Yin, L.H. Study on properties of single-phase high entropy alloys with FCC structure based on the empirical electron theory. *J. Alloys Compd.* **2022**, *896*, 162892. [CrossRef]
7. Xu, T.; Chen, Q.J.; Ji, L.; Zheng, Z.D.; Wang, K.; Liu, H.Y. BCC/B2 structure and dislocation strengthening behavior in high Ti content TiAlVCrNb high-entropy alloys. *J. Alloys Compd.* **2023**, *956*, 170179. [CrossRef]
8. Shi, J.; Zhao, Y.W.; Jiang, C.L.; Wang, X.; Zhang, Y.Z.; Zou, D.L.; Xu, H.Y.; Huang, H.; Luo, C. Development of single-phase bcc UHfNbTi high-entropy alloy with excellent mechanical properties. *Mater. Lett.* **2022**, *307*, 130822. [CrossRef]
9. Takeuchi, A.; Amiya, K.; Wada, T.; Yubuta, K.; Zhang, W. High-entropy alloys with a hexagonal close-packed structure designed by equi-atomic alloy strategy and binary phase diagrams. *JOM* **2014**, *66*, 1984–1992. [CrossRef]
10. Lužnik, J.; Koželj, P.; Vrtnik, S.; Jelen, A.; Jagličić, Z.; Meden, A.; Feuerbacher, M.; Dolinšek, J. Complex magnetism of Ho-Dy-Y-Gd-Tb hexagonal high-entropy alloy. *Phys. Rev. B* **2015**, *92*, 22420122. [CrossRef]
11. Ye, Q.L.; Zhang, Z.F.; Wang, Q.Y.; Xu, X.Y.; Wang, K.S.; Zhao, J.Q.; Xu, B.; Zhang, J.; Liu, D.D.; Deng, Y.D.; et al. Promoting nanoscale deformation twinning through FCC phase decomposition in $AlCoCrFeMo_{0.05}Ni_2$ high entropy alloy. *J. Alloys Compd.* **2024**, *985*, 174086. [CrossRef]
12. Otto, F.; Dlouhý, A.; Pradeep, K.G.; Kuběnová, M.; Raabe, D.; Eggeler, G.; George, E.P. Decomposition of the single-phase high-entropy alloy CrMnFeCoNi after prolonged anneals at intermediate temperatures. *Acta Mater.* **2016**, *112*, 40–52. [CrossRef]
13. Li, B.; Ming, K.S.; Bai, L.C.; Wang, J.; Zheng, S.J. Tailoring Mechanical and Electrochemical Properties of the $Cr_{15}Fe_{20}Co_{35}Ni_{20}Mo_{10}$ High-Entropy Alloy via the Competition between Recrystallization and Precipitation Processes. *Coatings* **2022**, *12*, 1032. [CrossRef]
14. Li, Z.Y.; Wang, X.H.; Huang, Y.Y.; Xu, Z.X.; Deng, Y.L.; Jiang, X.Y.; Yang, X.H. Microstructure, Mechanical Property, and Wear Behavior of NiAl-Based High-Entropy Alloy. *Coatings* **2023**, *13*, 1737. [CrossRef]
15. Chen, S.T.; Tang, W.Y.; Kuo, Y.F.; Chen, S.Y.; Tsau, C.H.; Shun, T.T.; Yeh, J.W. Microstructure and properties of age-hardenable $Al_xCrFe_{1.5}MnNi_{0.5}$ alloys. *Mater. Sci. Eng. A.* **2010**, *527*, 5818–5825. [CrossRef]
16. Tsao, L.C.; Chen, C.S.; Chu, C.P. Age hardening reaction of the $Al_{0.3}CrFe_{1.5}MnNi_{0.5}$ high entropy alloy. *Mater. Des.* **2012**, *36*, 854–858. [CrossRef]
17. Ren, B.; Liu, Z.X.; Cai, B.; Wang, M.X.; Shi, L. Aging behavior of a $CuCr_2Fe_2NiMn$ high-entropy alloy. *Mater. Des.* **2012**, *33*, 121–126. [CrossRef]
18. Zhao, R.F.; Ren, B.; Zhang, G.P.; Liu, Z.X.; Zhang, J.J. Phase transition of as-milled and annealed CrCuFeMnNi high-entropy alloy powder. *Nano* **2018**, *13*, 1850100. [CrossRef]
19. Ren, B.; Zhao, R.F. Elemental synergistic effect in $Co_xCrCuFeMnNi$ high-entropy alloys and its influence on phase and magnetic properties. *J. Mater. Res. Technol.* **2023**, *23*, 2542–2556. [CrossRef]
20. Mohanty, S.; Gurao, N.P.; Biswas, K. Sinter ageing of equiatomic $Al_{20}Co_{20}Cu_{20}Zn_{20}Ni_{20}$ high entropy alloy via mechanical alloying. *Mater. Sci. Eng. A.* **2014**, *617*, 211–218. [CrossRef]
21. Mohanty, S.; Gurao, N.P.; Padaikathan, P.; Biswas, K. Ageing behaviour of equiatomic consolidated $Al_{20}Co_{20}Cu_{20}Zn_{20}Ni_{20}$ high entropy alloy. *Mater. Charact.* **2017**, *129*, 127–134. [CrossRef]
22. Yao, X.F.; Wang, W.H.; Qi, X.L.; Lv, Y.K.; Yang, W.; Li, T.Y.; Chen, J. Effects of heat treatment cooling methods on precipitated phase and mechanical properties of CoCrFeMnNi–$Mo_5C_{0.5}$ high entropy alloy. *J. Mater. Res. Technol.* **2024**, *29*, 3566–3574. [CrossRef]
23. Xiong, K.; Huang, L.; Wang, X.; Yu, L.; Feng, W. Cooling-rate effect on microstructure and mechanical properties of $Al_{0.5}CoCrFeNi$ high-entropy alloy. *Metals* **2022**, *12*, 1254. [CrossRef]
24. Yu, H.Y.; Fang, W.; Chang, R.B.; Bai, X.; Zhang, X.; Liu, B.X.; Jiang, Y.F.; Yin, F.X. Effects of annealing temperature and cooling medium on the microstructure and mechanical properties of a novel dual phase high entropy alloy. *Mater. Charact.* **2020**, *163*, 110291. [CrossRef]
25. Faraji, A.; Farvizi, M.; Ebadzadeh, T.; Kim, H.S. Microstructure, wear performance, and mechanical properties of spark plasma-sintered AlCoCrFeNi high-entropy alloy after heat treatment. *Intermetallics* **2022**, *149*, 107656. [CrossRef]
26. Wang, W.R.; Wang, W.L.; Yeh, J.W. Phases, microstructure and mechanical properties of $Al_xCoCrFeNi$ high-entropy alloys at elevated temperatures. *J. Alloys Compd.* **2014**, *589*, 143–152. [CrossRef]

27. Salloom, R.; Joshi, S.S.; Dahotre, N.B.; Srinivasan, S.G. Laser surface engineering of B4C/Fe nano composite coating on low carbon steel: Experimental coupled with computational approach. *Mater. Des.* **2020**, *190*, 108576. [CrossRef]
28. Zhao, R.F.; Liang, Y.C.; Ren, B.; Jiang, A.Y.; Liu, J.X.; Zhang, B.F. Effect of elemental synergism on the mechanical behavior of CoCrCuFeMnNi high-entropy alloy system. *Met. Mater. Int.* **2023**, *30*, 1505–1512. [CrossRef]